A Fully Inkjet-Printed Wireless and Chipless Sensor for CO_2 and Temperature Detection

Arnaud Vena, *Member, IEEE*, Lauri Sydänheimo, *Member, IEEE*,
Manos M. Tentzeris, *Fellow, IEEE*, and Leena Ukkonen, *Member, IEEE*

***Abstract*— A study on a low-cost wireless fully inkjet-printed chipless sensor on a flexible laminate with three different inks is presented. It is based on two split ring resonator 90° oriented between each other to allow for independent responses on two polarizations. A deposit of a polymer/single walled carbon nanotube composite ink is used to allow for the detection of CO_2 as well as temperature. In this paper, it is shown that the inkjet printing of a polymer-based coating on top of the sensing/reactive deposit can significantly reduce the sensitivity to CO_2, whereas the temperature sensitivity stays at same. Simulations and experimental results verify the repeatability of this topology.**

***Index Terms*— Chipless sensor, RFID, gas, temperature, inkjet-printing, carbon nanotubes.**

I. Introduction

THE real-world implementation of Internet-of-Things (IoT) and Ambient Intelligence systems has necessitated the development of novel reliable low-cost wireless solutions in order to sense and communicate information for everything and everywhere. Radio frequency Identification (RFID) technology seems to be the ideal candidate for this key role. An RFID tag or or an RFID-enabled sensor is cheap, reliable and can be detected at several meters with no battery, while it embeds a significant memory that can be read and written remotely. The most popular RFID-enabled applications include pallet tracking, identification of persons in urban transportation networks, and antitheft systems. Adding sensing functions to RFID tags has been investigated for several years [1], [2] and it has been proven that various physical parameters as well as chemical substances can be detected with RFID tags with or without an additional analog to digital converter (ADC). The former one can provide an accurate value of the sensed parameter at the expense of higher-energy consumption, whereas the second category can be mainly used as threshold sensors because usually the surrounding environment interferes with the measurement. To track the quality of the air, or the quality of pharmaceutics or food products, the price of sensors has to be even lower than the current unit cost of a chip-enabled RFID tag that is 0.1 $. For this kind of application, the chipless RFID technology [3]–[10] may reduce dramatically the sensor's unit cost. Because it requires no integrated circuit (IC), a chipless sensor [11]–[18] can be realized from scratch, only using a printer. The identifier (ID) as well as the sensed information relies upon the analysis of its electromagnetic (EM) signature in the frequency domain or in the time domain. Like an optical barcode, its cost is mainly linked to the cost of the ink and the printing process, as well as the substrate that can be even plastic or paper. We can find numerous state-of-the-art designs of chipless sensors for gas [11], [12], temperature [13], [14], humidity [16] or strain [17], but few of them show a full implementation of an entirely printed wireless sensor as well as a study about their reproducibility.

The present paper aims to study the realization of a printed CO_2 and temperature sensor using different commercial inks. The sensitivity of the chipless sensor is due to the deposition of a composite polymer/single-walled carbon nanotube (SWCNT) ink. Indeed, it has been shown that CNT and graphene sheets present a strong sensitivity to various gases [19]–[22] and other physical parameters. In a previous work [18], a simple setup verified the sensitivity of the proposed design to the smoke which embeds various physical parameters. This paper aims to study in more depth, and to understand the behavior of the sensor when subject separately to CO_2, and to a temperature variation. Moreover, a parametric study, concerning the number of layers of the sensitive material, is carried out to optimize the performance of the sensor. Several samples have been realized to study its reproducibility. For selectivity purposes, we study the effect of a top coating layer with a polymer based ink, on the sensitivity of the sensor both in temperature and CO_2.

In Section II, we present the design of the chipless sensor (see Fig. 1) and its operation principle. In Section III, a study on the selectivity of the sensor for both CO_2 and temperature is provided and validated by wireless measurements. Then before concluding, in Section IV, we investigate a possible way to separate the effect of temperature and CO_2 variations on the RCS value of the sensor through the use of a coating layer on top of the sensitive material.

Manuscript received April 12, 2014; revised June 23, 2014; accepted June 26, 2014. Date of publication July 7, 2014; date of current version November 5, 2014. This work was supported in part by the Finnish Funding Agency for Technology and Innovation, in part by the Academy of Finland, in part by the Centennial Foundation of Finnish Technology Industries, in part by the New Energy and Industrial Technology Development Organization in Japan, and in part by the National Science Foundation. The associate editor coordinating the review of this paper and approving it for publication was Prof. M. R. Yuce.

A. Vena, L. Sydänheimo, and L. Ukkonen are with the Tampere University of Technology, Tampere 33720, Finland (e-mail: arnaud.vena@tut.fi; lauri.sydanheimo@tut.fi; leena.ukkonen@tut.fi).

M. M. Tentzeris is with the Georgia Institute of Technology, Atlanta, GA 30332-250 USA (e-mail: etentze@ece.gatech.edu).

Color versions of one or more of the figures in this paper are available online at http://ieeexplore.ieee.org.

Digital Object Identifier 10.1109/JSEN.2014.2336838

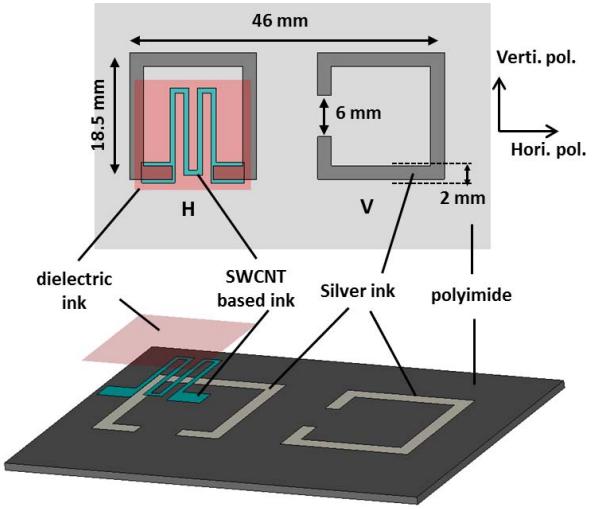

Fig. 1. View of the fully inkjet-printed dual polarized sensor with the help of three different inks.

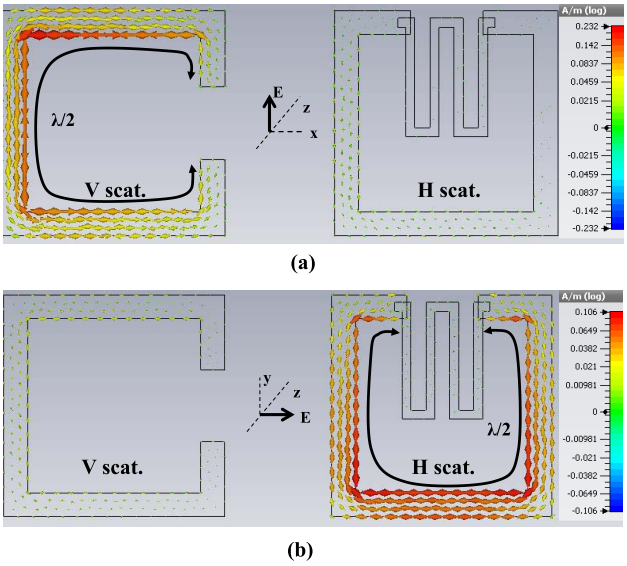

Fig. 2. Surface current distribution at 2.4 GHz for the dual polarized SRR based sensor (a) in vertical polarization and (b) in horizontal polarization.

II. Design and Principle

A. Radiation of a Dual Polarization SRR

The basic principle of a chipless RFID sensor is very similar to the concept of a chip RFID enabled sensor having no integrated ADC. The detection of a physical parameter relies upon the variation of the conductivity or the permittivity of a sensitive material. These changes induce modifications on the radar cross section (RCS) of the tag as a function of the frequency. As a result, we can detect both resonant frequency and magnitude shifts of some peaks in the spectral response of the tag. This sensor has been designed to provide two separate responses using two orthogonal responses. The EM response of one polarization can be used to extract the sensed information, whereas the response of the other one is used as a reference response (for calibration) as well as for identification coding. This concept already introduced in [18] for smoke detection is taken as it is for this new study. Figures 2(a) and (b) show surface currents on both scatterers when subjected to an incident plane wave vertically and horizontally polarized, respectively. As we can see, only one scatterer is excited at a given polarization, so this provides a very good EM response isolation between each scatterer. As a result, the variation of the magnitude of the sensing scatterer does not affect the magnitude of the reference scatterer.

The dimensions of the scatterers have been optimized to operate in the band 2.4 GHz to 2.5 GHz. The split ring resonators (SRR) are squared-shaped with a side length of 18.5 mm. The gap between the two arms of the SRR is 6 mm long that is a tradeoff between the size, the bandwidth of the resonant peak, and its EM response strength. The width of the SRR is 2 mm to allow for a low strip resistance that is beneficial for the RCS magnitude. Indeed, a narrower strip width may lead to a performance deterioration regarding the conductivity of a printed strip based silver ink that is lower than etched bulk copper. As shown in Fig. 2(a) and (b), a separation of 9 mm between the two scatterers allows for a sufficiently good decoupling of their EM responses (cross-polarization isolation of -15 dB at minimum). A smaller separation distance would have led to a larger bandwidth for resonant peaks in both polarizations, as well as weaker cross-polarization isolation.

B. Coding and Reference Scatterer

The scatterer denoted "V" in Fig. 1 is used for coding and calibration purposes. This means that its RCS response does not change as a function of the time when subject to time-varying gas concentrations. This scatterer is not loaded with a sensitive material. The RCS magnitude of the peak can be used to calibrate the sensed information extracted from the orthogonal polarization. Indeed, a normalization of the RCS magnitude of the sensed parameter by that of the reference scatterer (that will not likely change) allows getting a result independent from the reading distance as proved by equation (1) to (4) in the ideal case of free-space propagation. The radar equations (1) and (2) for both polarizations depend on the gain *Gt*, *Gr* of the transmitting and receiving antennas, the distance R and the RCS σ_{VV}, σ_{HH} in vertical and horizontal polarization, respectively. Assuming that σ_{VV} is constant and σ_{HH} is linked to σ_{VV} by a coefficient K as in (3) which depends on the CO_2 concentration and other parameters such as the temperature, we can obtain (4). This last equation says that the ratio of the received power levels $\mathrm{Pr}_{HH}/\mathrm{Pr}_{VV}$, in both polarizations is equal to the coefficient K whatever the distance, and for a constant transmitted power *Pt*. Practically, the maximum distance of detection can be calculated with the modified radar equation (5) for a given equivalent isotropic radiated power (EIRP) of $Pt^{eirp} = 36$ dBm (ISM band at 2.45 GHz) and a minimum RCS value σ_{min}, chosen to -35 dBsm for this design. As an example with a 6 dBi receiving antenna gain *Gr* and a minimum received power

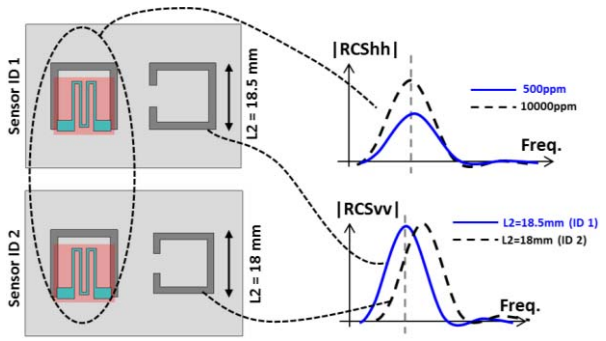

Fig. 3. Basic principle of the dual polarized sensor. Vertical polarization is used for the identification whereas horizontal polarization is used for sensing.

of $Pr^{min} = -74$ dBm, the detection range is $R^{max} = 5.55$ m.

$$\frac{\mathrm{Pr}_{VV}}{pt} = \frac{G_t G_r \lambda^2 \sigma_{VV}}{(4\pi)^3 R^4} \tag{1}$$

$$\frac{\mathrm{Pr}_{HH}}{pt} = \frac{G_t G_r \lambda^2 \sigma_{HH}}{(4\pi)^3 R^4} \tag{2}$$

$$\sigma_{HH} = K_{\langle CO_2, T°C\rangle} \times \sigma_{VV} \tag{3}$$

$$\frac{\mathrm{Pr}_{HH}}{\mathrm{Pr}_{VV}} = K_{\langle CO_2, T°C\rangle} \tag{4}$$

$$\mathrm{R}^{max} = \sqrt[4]{Pt^{eirp} \times Gr \frac{\lambda^2}{(4\pi)^3 \times Pr^{min}} \sigma_{min}}. \tag{5}$$

For identification coding purposes, a frequency shift coding technique can be used as shown in Fig. 3. Depending on the location of the peak in the frequency span between 2.4 GHz and 2.5 GHz, a different ID can be detected. For the proposed design when the length of the coding scatterer L2 is 18.5 mm, the resonant frequency is close to 2.4 GHz giving the ID 1. Whereas, for L2 = 18 mm, the frequency is close to 2.5 GHz giving the ID 2. Simulation results for a length L2 between 18mm and 18.5mm are plotted in Fig. 4. The observation of the frequency span between 2.4 GHz and 2.5 GHz is enough to distinguish the three configurations.

It is to be noted that two sensors close to each other cannot perform in a satisfactory way as it is the common case for numerous chipless systems. However, the bandwidth of each sensor that is quite large does not permit the detection of two sensors simultaneously in the ISM band at 2.4GHz, but one can consider using the ISM band at 5.8GHz for simultaneous interrogations. Possible techniques to separate the chipless tag's response are presented in [23]. For example spatial separation with the help of a narrow beam reader antenna is one of the best solution to separate tag's responses.

C. CNT Loaded Scatterer for Sensing

The scatter denoted "H" in Fig. 1 is used for sensing. To make it sensitive, a printed strip based on a SWCNT/PEDOT-PSS composite ink [24] is inserted within the gap of the SRR. According to some previous characterizations, we found that the conductivity of the deposit is the main varying parameter when subject to a gas or a temperature change, thus it can be modeled by a variable resistor. In the gap area,

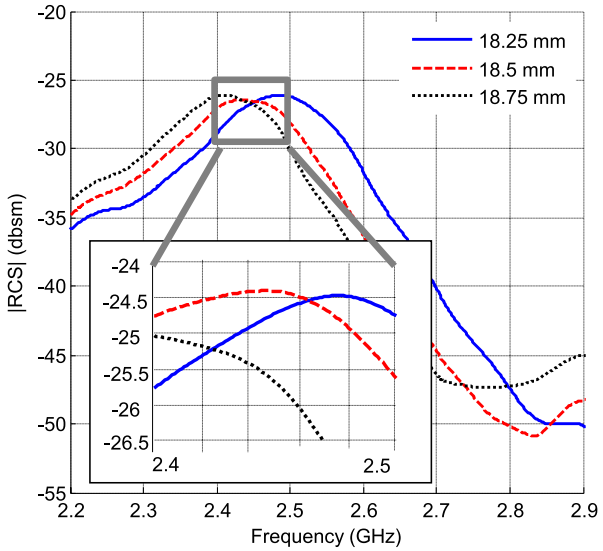

Fig. 4. RCS simulation results for various values of length L2 between 18 mm and 18.5 mm.

the impedance is the highest possible, so that a strong deviation can be observed even if the bridging resistance of the deposit has a high value, which is the case for this CNT-based ink. To maximize the sensitivity of the sensor, we can assume that the reactive surface has to be the largest possible. On the other hand, we cannot deposit a large resistive patch in the gap to avoid cancelling the first resonant mode of the scatterer. Indeed, in this configuration, the resistive strip can be considered as a resistor in parallel of a resonant circuit, so if the bridging resistance goes very low, the quality factor of the resonant peak fall down, and we cannot observe it anymore. We inserted the sensitive strip inside the SRR as shown in Fig. 1 so that most of the surface is covered within this area. We seek to get the longest path to cover the highest surface within the SRR. For that reason, the sensitive strip features a meander shape. The ratio between the length of the path and its width is chosen so that the nominal bridging resistance is achieved according to the sensitivity study that follows. This gives a strip width of 0.75 mm and a path length of 54 mm. Moreover, to ensure a good electrical contact between the sensitive strip and the printed SRR, the SWCNT/PEDOT-PSS based strip overlaps the silver strip on each side of the gap, with a surface of 4.5×2 mm^2 (see Fig. 1).

To find the nominal bridging resistance maximizing the linear and the logarithmic RCS deviation we carried out a parametric study with the help of CST Microwave Studio (CST MWS) varying the sheet resistance of the sensitive strip between 10 Ω/sq and 100000 Ω/sq. We modeled the sensitive strip with a zero thickness sheet made of a material defined as an ohmic surface under CST MWS.

Figure 5(a) and (b) show the simulated RCS responses for various sheet resistances, for the vertical polarization and the horizontal polarization, respectively. The Fig. 5(a) confirms the good decoupling between the two polarizations, because the modification of the sheet resistance of the sensitive deposit has no effect on the vertically polarized response. On the other hand, we can observe a significant magnitude

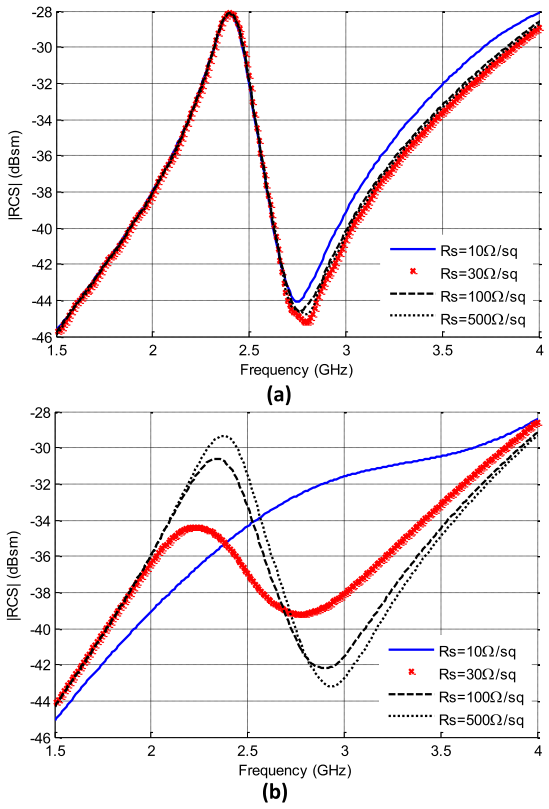

Fig. 5. RCS simulations results obtained as a function of the sheet resistance of the SWCNT deposit for (a) the vertical polarization and (b) the horizontal polarization.

variation on the horizontally polarized response. Figure 6(a) shows the linear and the logarithmic variation of the RCS as a function of the sheet resistance in logarithmic scale. To maximize the sensitivity due to the sheet resistance variation, we have to choose a nominal value of the curve when the slope is at its maximum. Figure 6(b) shows the derivatives of the curves of Fig. 6(a). According to these last figures, we observe a maximum linear variation between 200 Ω/sq and 10000 Ω/sq and a maximum logarithmic variation between 200 Ω/sq and 700 Ω/sq. Thus, a nominal sheet resistance value close to 450 Ω/sq is a good choice to maximize the magnitude variation of the RCS.

D. Material and Realization Process

As a proof-of-concept prototype, the sensors shown Fig. 7, are inkjet printed on a flexible polyimide laminate with 50 μm thickness. The permittivity is 3.5 and the loss tangent tanδ = 0.0027. We use the inkjet printer Dimatix DMP-2831 for material deposition. To create the high conductivity strip, we used silver ink, Harima Nanopaste. We printed two layers at a resolution of 635 dpi followed by a sintering at 150 °C for one hour to get a thickness close to 2 μm. The achieved sheet resistance is close to 0.5 Ω/sq.

For the sensitive conducting strip we use a SWCNT/ PEDOT-PSS composite ink [24], [25]. This sensitive material is printed with a resolution of 1693 dpi after having been sonicated during 30 min at 30 °C. Sintering is not required after printing, and the ink dries quickly at an ambient temperature.

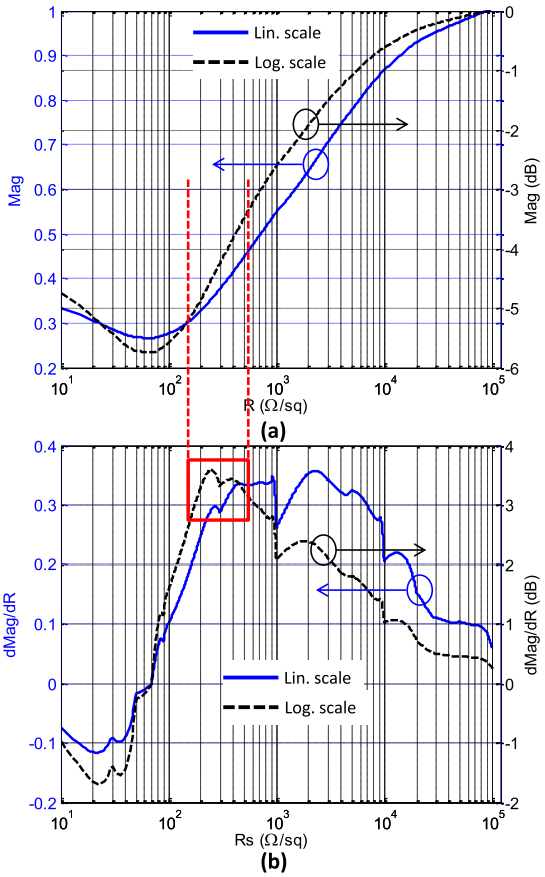

Fig. 6. (a) Linear and logarithmic relative magnitude of the resonant peak as a function of the sheet resistance of the sensitive strip. (b) Linear and logarithmic derivative of the relative magnitude of the resonant peak as a function of the sheet resistance of the sensitive strip.

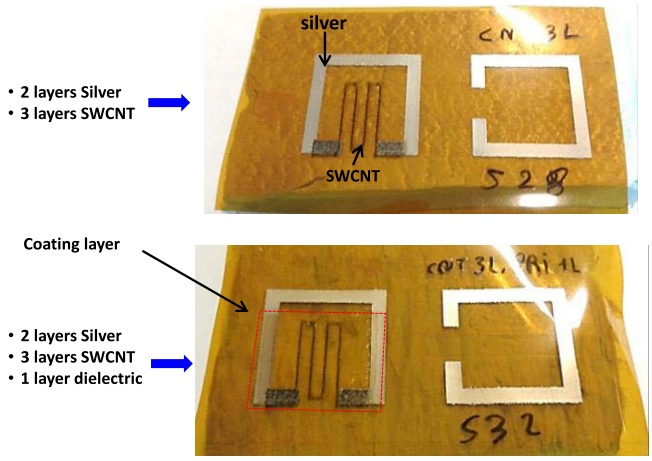

Fig. 7. View of the realized fully inkjet-printed sensors on polyimide substrate. The sensor at the bottom of the figure has an additional coating layer (quite transparent) on top of the sensitive deposit.

After drying, we measured a DC resistance R_{DC} of 72k, 32.4k and 21.6k respectively for one, two and three layers. Using (6), with w and L, the width (w =0.75 mm) and the length (L = 54 mm) of the strip we can obtain the corresponding sheet resistance R_S close to 1000 Ω/sq, 450 Ω/sq and 300 Ω/sq.

$$\mathrm{R}_S = \mathrm{R}_{DC} \times \frac{w}{L} \tag{6}$$

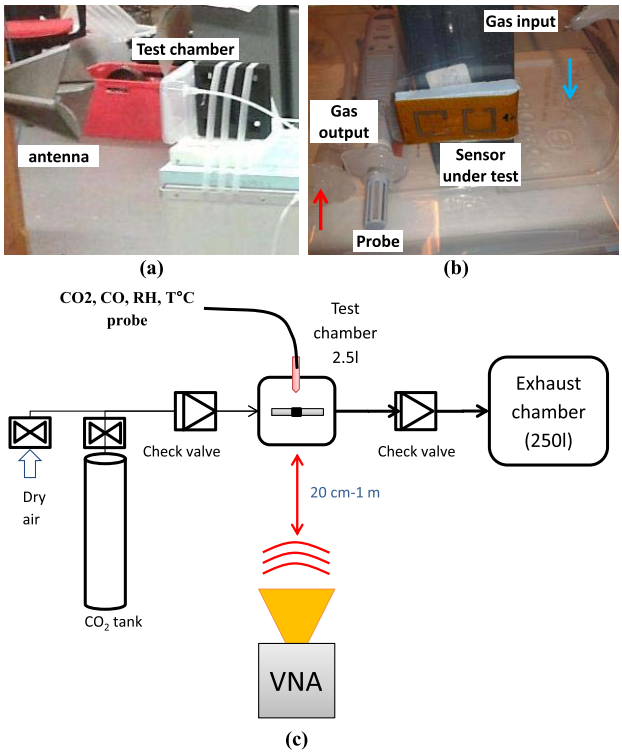

Fig. 8. Measurement set-up. (a) View of the antenna front of the test chamber. (b) View of the test chamber. (c) Description of the set-up for gas measurement.

III. Study on the Sensitivity of CNT-Based Sensor for Several Physical Parameters

A. Description of the Setup

We realized nine samples for the design shown in Fig. 1 and Fig. 7. The dimensions of the SRR and the sensitive strips are kept to the same values for all samples. The varying parameters are the number of layers of the CNT based strip, between two and four layers. The measurement set-up of the Fig. 8 is used to carry out the CO_2 measurement. A sealed plastic box is used as a test chamber, big enough to contain the sensor as shown in Fig. 8 (b). The chamber has an input inlet and an output inlet with check valves to avoid the composite gas flowing back. Either dry air (10% of relative humidity) or a specific gas can be injected in the test chamber. According to a sensitivity study of CNTs in [19], several gases can be detected such as NO_2, NH_3, and CO_2. In this paper we focus on studying the sensitivity of the SWCNT deposit to CO_2 only. The injection of CO_2 is performed by manual quick discharge. Each injection saturates the concentration inside the chamber at a level close to 20000 ppm. A probe Delta Ohm HD37AB17D measures the concentration of the CO_2 and records the temperature and the relative humidity (RH), at the same time. A wideband dual polarized ridged horn antenna ETS Lindgren 3164-04 having a gain between 9 dBi and 12 dBi from 3 GHz to 6 GHz is placed at 20 cm away from the test chamber. The ports of this antenna are connected to those of a vector network analyzer (VNA) Agilent PNA E8358A. The scattering parameters S11 and S22 allow for the extraction of the vertically polarized and the horizontally polarized EM response, respectively. It is noteworthy that measurements have been carried in an indoor environment, which implies multi-path effects and interferences with surrounding wireless communications. To address this problem, we used an averaging filter as well as a time gating filter on the raw measurement results. The extraction of the EM response of the tag is not direct and requires two additional measurements as explained below:

1) The measurement of the background with no tag, to remove the echoes from surrounding objects.
2) The measurement of a reference object having a known RCS to de-embed the gain non-uniformity of the reader antenna over the frequency range. For this study, we use a 5x5 cm^2 flat squared metallic plate.

Based on those measurements we can apply equation (7) and (8) to extract the RCS of the sensor in vertical and horizontal polarization denoted σ_V and σ_H, respectively.

$$\sigma_v = \left[\frac{S11_{sens} - S11_{empty}}{S11_{ref} - S11_{empty}}\right]^2 \sigma_{Vref} \tag{7}$$

$$\sigma_H = \left[\frac{S22_{sens} - S22_{empty}}{S22_{ref} - S22_{empty}}\right]^2 \sigma_{Href} \tag{8}$$

$$\sigma_{ref} = \frac{4\pi A^2}{\lambda^2}. \tag{9}$$

The terms $S11_{sens}$, $S11_{empty}$ and $S11_{ref}$ are the recorded scattering parameters on the port 1 of the VNA for the sensor measurement, the background measurement and the reference object measurement, respectively. Similarly, the variables $S22_{sens}$, $S22_{empty}$ and $S22_{ref}$ are the recorded scattering parameters on the port 2 of the VNA for the aforementioned measurements. The terms σ_{Vref} and σ_{Href} are the theoretical values of RCS for the reference scatterer. These parameters can be either extracted through simulation or based on the analytical formula (9) given for a flat plate [27], with A the surface of the plate, provided that the detection distance is far enough.

For all measurements, the transmitted power is 0 dBm between 2.2 GHz and 2.6 GHz, and the intermediate filter (IF) of the VNA is set to 100 Hz, giving a noise floor low enough to be compatible with a measurement at 20 cm. A lower value for the IF bandwidth will be preferred to enable higher reading distances. For this work we use an experimental setup based on a VNA to extract the RCS of the sensors that is not a cheap solution. However, for a real application, this setup could be replaced by a low-cost dedicated reader as it has been demonstrated in [28] for a frequency-domain approach, and in [29] for a time-domain approach.

B. Study on the Effect of the Number of CNT-Based Ink Layers on the Sensitivity to CO_2

We study first the effect of the number of layers on the sensitivity of the sensor. We realized three samples having two, three and four layers of CNT ink to create the sensitive strip. Each sample is subjected to UV light during 10 min just before measurement with CO_2 gas.

Figure 9(a) and (b) show the evolution of the RCS response for the tag with two layers of CNT-based ink, for both polarizations, when subject to CO_2. Additionally, Figs. 10 and 11

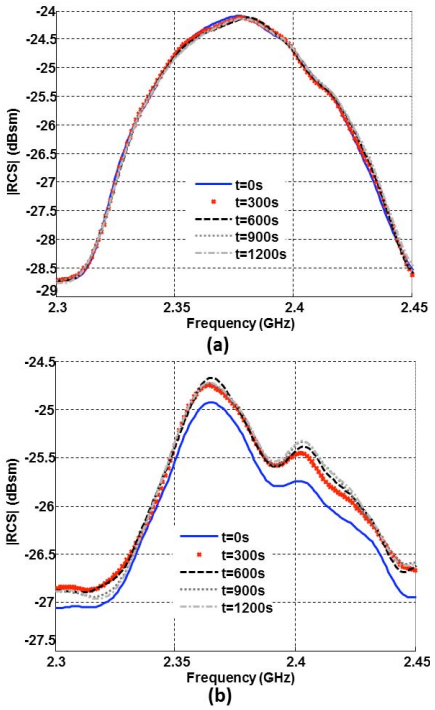

Fig. 9. RCS measurement results of the 2 layers based sensor for several recording times when CO_2 is injected inside the test chamber: (a) for the vertical polarization and (b) for the horizontal polarization correlated with the resonator loaded with the sensitive deposit.

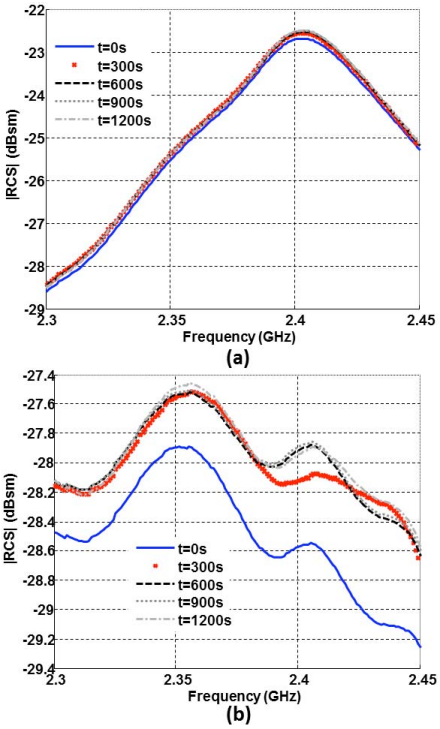

Fig. 10. RCS measurement results of the 3 layers based sensor for several recording times when CO_2 is injected inside the test chamber: (a) for the vertical polarization and (b) for the horizontal polarization correlated with the resonator loaded with the sensitive deposit.

show the same results for three and four layers, respectively. Meanwhile, the relative humidity (RH) varies very little (between 15% and 20%), and the temperature stays at the same value (around 21 °C). We can remark that the magnitude of

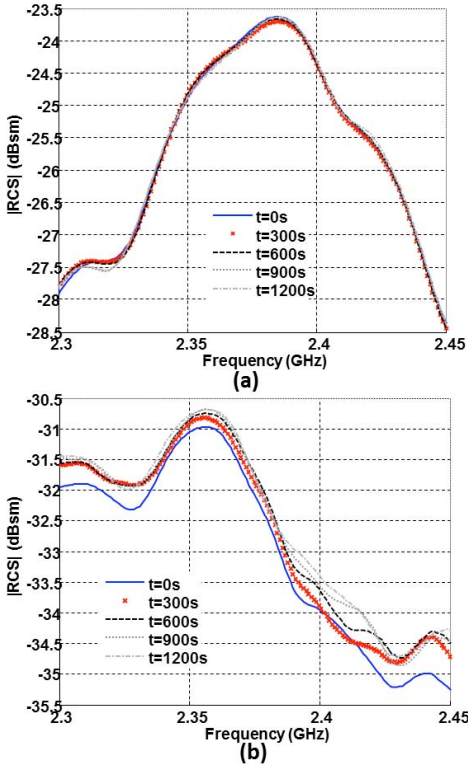

Fig. 11. RCS measurement results of the 4 layers based sensor for several recording times when CO_2 is injected inside the test chamber: (a) for the vertical polarization and (b) for the horizontal polarization correlated with the resonator loaded with the sensitive deposit.

the EM response of the scatterer loaded by the sensitive strip varies more significantly than the unloaded scatterer in each case. In Fig. 9(b) and in Fig. 10(b) we can see the apparition of a smaller peak at higher frequency. This unexpected shape is most likely due to the residual echoes (even after the calibration) from the wall of the sealed plastic box. Indeed, those echoes are hard to cancel because the sealed box is in the same phase plane that the sensor to detect. To sense the variation of CO_2 we can monitor the magnitude variation at the dominant resonant peak as a function of the acquisition time as plotted in Fig. 12(b) for the three configurations. The plotted magnitude is normalized by the initial value before injection of gas.

The number of ink layers modifies the bridging resistance that effectively determines the initial RCS level before the exposure to gas. Thus to compare the sensitivity achieved as a function of the number of ink layers, one can use the normalized RCS variation relative to the no exposure case as in Fig. 12(b).

It is noteworthy that the curves showing the recorded concentration of CO_2 as a function of the time, are very close to each other for the three samples (see Fig. 12(a)). The RCS value changes very rapidly (after 150-200 sec) and converges to its maximum value quickly afterwards, while it never returns to the "no-gas" value because the CO_2 molecules are trapped inside the SWCNT lattices. For a variation between 500 ppm and 20000 ppm, 90 % of the maximum magnitude shift is attained with a response time approximately of 30 s at 21 °C (to compare, a same order value of 45 s is achieved in [20]

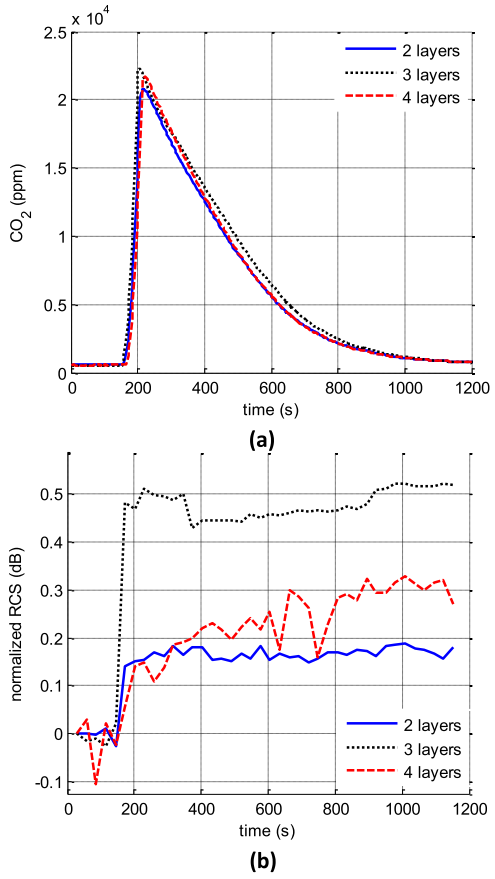

Fig. 12. (a) Recorded CO_2 concentration with the probe for the three samples having various layers. The temperature is almost constant (close to 21 °C). (b) Normalized magnitude of the resonant peak (at 2.38 GHz) for the horizontally polarized EM response as a function of the time for various layers of SWCNT based ink. A short discharge of CO_2 is injected 180 s after the beginning of the test.

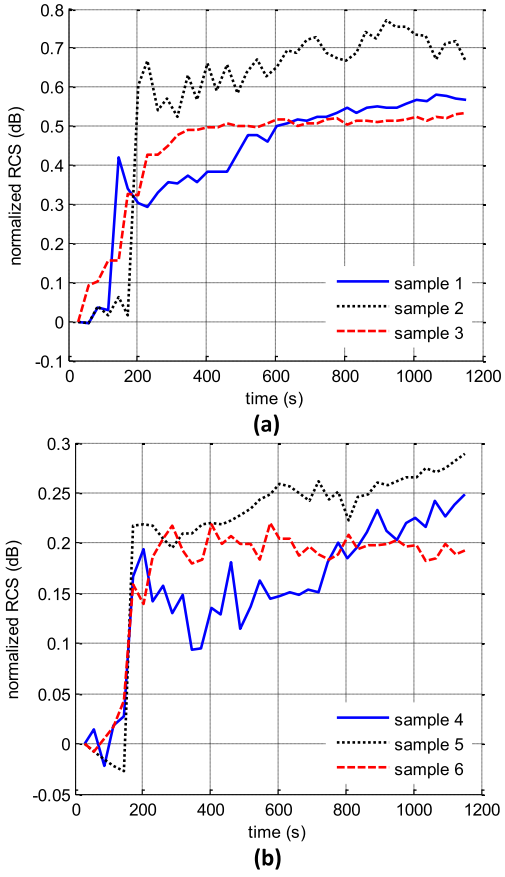

Fig. 13. Normalized magnitude of the resonant peak (at 2.38 GHz) for the horizontally polarized EM response as a function of the time for various samples: (a) with no coating and (b) with dielectric coating. A short discharge of CO_2 is injected 180 s after the beginning of the test.

at 43 °C). Thus, these sensors could be most likely used as threshold sensors ("green/red" event-detection sensor) instead of reversible linear sensors. A possible way to reset the sensor to its initial state should be to expose it to UV light during a long time as in [19] but this is an issue outside the scope of this paper.

According to Fig. 12(b), the sensor having three layers of CNT-based ink gives the best sensitivity with 0.5 dB to compare with 0.3 dB and 0.2 dB for four and two layers, respectively. This confirms the result of the sensitivity study (see Fig. 6) in section II.D saying that for this configuration, and with this CNT-based ink, three layers are a good choice to maximize both the linear and the logarithmic variation.

C. Reproducibility Measurement for CO_2 Detection

Based on the previous study, we know that three layers allow getting the highest sensitivity. Thus, we realized three similar samples and carried out new CO_2 measurements for a reading distance of 20 cm. We extracted the magnitude for the resonant peak in horizontal polarization, normalized by its initial value, as a function of the time for each sample as shown in Fig. 13(a). The curve shape is the same for the tree samples. We observe a quick rise of the RCS followed by a smooth slope converging to the final value from 200 s to the end of the experience. We can see that the maximum variation between the beginning and the end of test is contained between 0.52dB and 0.65dB for the three samples. The values obtained are close enough to be used as threshold sensors, showing that the realization of a large number of sensors with similar performance is feasible utilizing inkjet printing techniques. The small oscillations of the curves contained within ± 0.1 dB are most likely due to the small background changes over the measurement time. In terms of sensitivity, we can affirm that a level of 20000 ppm can be detected and gives an RCS variation of 0.5 dB.

D. Reproducibility Measurement for Temperature Detection

Another topic we are investigating in this paper is the sensitivity of the inkjet-printed sensors to the ambient temperature. For testing purposes, we used the same measurement setup shown in Fig. 8 except that we don't inject CO_2 but only hot air with the help of a hot air blower. The maximum temperature achieved is close to 60 °C with this technique. Figure 14 shows the temperature recorded by the probe during the test, for the three samples of Section III.C. We record the RCS response, as a function of the time. For the time $t = 0$ s, the hot air blower is turned off, and the measurement runs until the temperature get close to 27 °C. The time-evolution of the

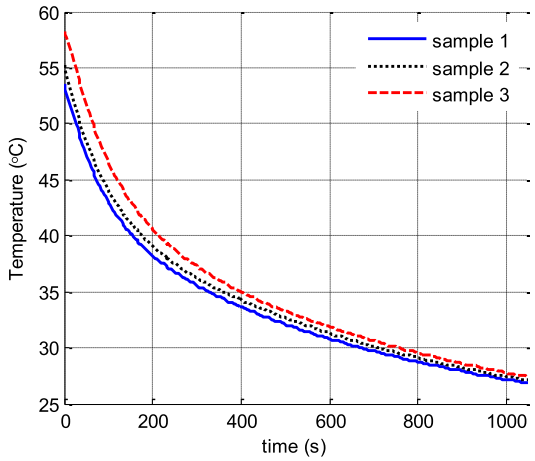

Fig. 14. Temperature recorded by the probe as a function of the time during the test of samples 1, 2 and 3. The CO2 concentration is constant (close to 500 ppm).

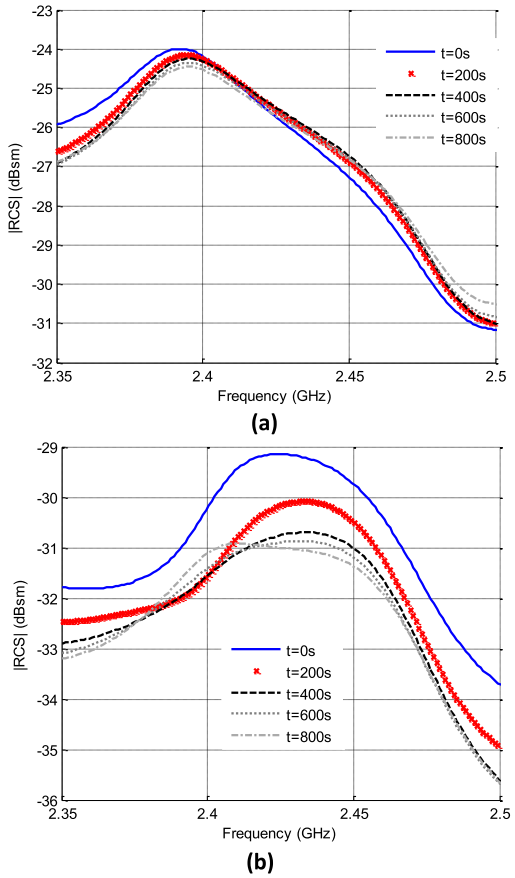

Fig. 15. RCS measurement results of the sensor 1 with no coating when temperature varies between 60 °C and 30 °C in the test chamber: (a) for the vertical polarization and (b) for the horizontal polarization correlated with the resonator loaded with the temperature-sensitive CNT.

RCS values over the frequency range of 2.35-2.5 GHz for the Sample 1 is shown in Fig. 15(a) and (b) for both polarizations, and Fig. 16(a) shows the extracted time evolution of the peak RCS magnitude value. The evolution of the RCS as a function of the time is very close to the recorded temperature curve, so that, there is an almost linear relationship between the RCS and the temperature. It can be seen that the maximum deviation is contained between 1.8dB and 2.2dB (for a variation of

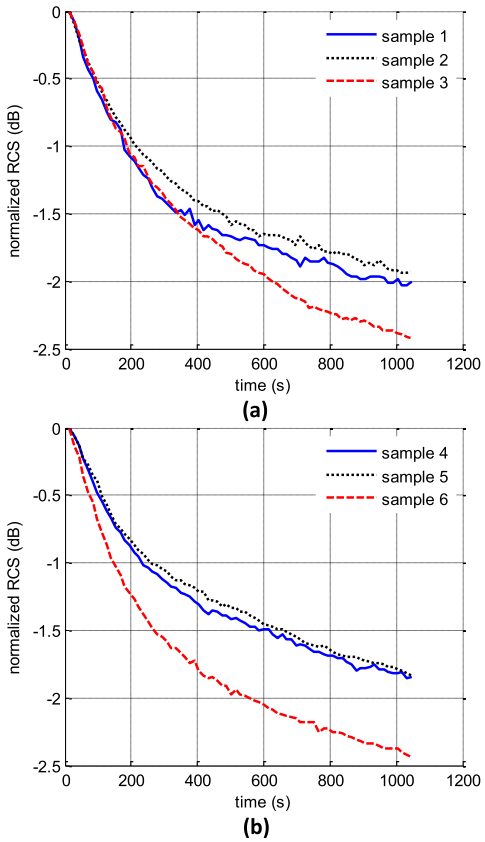

Fig. 16. Normalized magnitude of the resonant peak (at 2.4 GHz) for the horizontally polarized EM response as a function of the time for various samples: (a) with no coating and (b) with dielectric coating. The initial temperature is close to 60 °C and the final temperature is around 30 °C.

33 °C) in horizontal polarization for the three samples. This verifies the feasibility of the proposed sensor as a highly sensitive and highly repeatable temperature sensor with RCS values variations much larger than those for the CO2 detection. We can use this design as a temperature sensor having a reversible behavior, provided a calibration with a reference temperature. According to Figs. 14 and 16(a) the sensor shows a reproducible behavior between 60 °C and 35 °C (time 0 s to 400 s) with sensitivity of 1 dB for 16.6 °C. However, this simple design could be most likely used as a very cheap temperature sensor in applications, which do not require a high accuracy. For example, the sensor can be used to detect an excess temperature provided that the RCS level is compared in real time with a threshold value.

IV. Study of the Effect of Coating on the Sensitivity and Selectivity

The study that follows gives a potential solution to suppress the ambient-gas sensitivity of the reported temperature sensors, thus enhancing the temperature sensitivity. The idea is to print a layer of dielectric based ink on top of the sensitive area (Figs. 1 and 7) to filter the gas molecules, whereas keeping a good sensitivity to temperature variation. The dielectric is based on the PolyPrimer ink [25], [26] that can be polymerized with UV light. This ink has been chosen for its good overlay properties, as it allows making smoother the rough substrates, and for its low capacity of absorption of water. Thus, the

deposited dielectric layer is intended to be not porous. One layer is deposited with a resolution of 635 dpi on three new samples. Each sample is then exposed to UV light during two minutes. The measured thickness is 3 μm.

A. Reproducibility Measurement for CO_2 Detection

We carried out the CO_2 measurement following an identical procedure to section III.C, so that each sensor is exposed to UV light during 10 min just before measurement. The samples are then placed inside the test chamber, and pure CO_2 is injected. For the three samples, we can clearly see that the magnitude variation of the resonant peak has decreased from 0.5 dB previously to a value between 0.2 and 0.25 dB as shown in Fig. 13(b). However, the curve shape doesn't show any change and we still see a sharp step within the first 200 s followed by a nearly constant response. Thus, this confirms that the composite material based on four different polymers plays the role of a filter for CO_2 molecules. Increasing the number of layers will probably lead to an even higher attenuation of the peak magnitude variation.

B. Reproducibility Measurement for Temperature Detection

We now study the effect of the coating on the temperature sensitivity. Measurements are performed under the conditions listed in Section III.D, so that the RCS of the sensor is recorded during the temperature decrease from 60 °C to 30 °C. Figure 16(b) shows the RCS measurement results. We can observe a variation between 1.8 and 2.5 dB that is quite close to the one obtained without any coating. One can see a larger versatility on the response to compare with the case with no coating. This implies that a separate calibration is required for every different sensor. However, it seems that the coating superstrate does not affect the temperature sensitivity whereas the sensitivity to CO_2 is strongly attenuated as verified in the previous section. As a conclusion, with a simple surface treatment that it consists of adding a dielectric layer on top of the sensitive area, it is confirmed that that accurate temperature sensing with virtually no effect of ambient gas varying concentrations can be achieved.

V. Discussion on Performance and Practical Implementation

In this section we compare the proposed sensor amid similar wireless chipless sensing technologies and discuss several points in order to increase its performances.

A. Performance Comparison

In the Table I, we list a comparison of our proposed sensor with other previously reported wireless and/or passive sensors designed either for temperature or carbon dioxide monitoring. The main criterions evaluated are the sensitivity and the compatibility with printable electronics. According to the measurement results we get a RCS variation of 12.2% from 500 to 20000 ppm. Concerning the temperature, the RCS features a variation of 36.9% from 30 °C to 60 °C. Regarding the CO2 sensitivity, the performances reported in [20] using MWCNT are significantly lower featuring a 1% of permittivity change for a saturated atmosphere. The work reported in [21] shows a similar sensitivity with 0.33% of relative resistance variation for 369ppm (17.88% of resistance shift for 20000 ppm by extrapolation). The best sensitivity is obtained in [22] with 25% conductivity shift for 100ppm only. In this case the material used is a graphene sheet but according to the realization process the sensor cannot be printed as it is.

TABLE I
Performance Comparison of Passive Sensors

Ref.	Material	Printable	CO_2 Sensitivity	T°C Sensitivity
This work	SWCNT	Yes	12.2% (RCS) for 20000 ppm	36.9% (RCS) for 30°C
[20]	MWCNT	Yes	1% (Permittivity) for 100% CO_2	-
[21]	MWCNT	Yes	0.33% (resistance) for 369ppm	-
[22]	Graphene sheet	No	25% (conductance) for 100 ppm	
[13]	Au/Si	No	-	498MHz/°C
[14]	µfluid	No	-	9dBsm (87% RCS)for 20°C
[15]	BST	Yes	-	3.1MHz/°C or 6.7% (frequency) for 65°C

Concerning the temperature sensors, best sensitivity values are achieved by the MEMS based [13], and microfluidic based [14] chipless sensors. The design reported in [15] has a lower sensitivity but it presents some advantages such as to be compatible with printing techniques like the sensor proposed in this article. To compare with the 36.9% of magnitude variation obtained in this work for 30 °C of temperature variation the sensitivity achieved in [15] is lower. However it presents some advantages such as the detection reliability in a practical environment (frequency shift, use of two antennas operating in orthogonal polarizations). This last point should be improved for our current design.

B. Toward the Practical Implementation of the Sensor

We give thereafter some possible solutions in order to practically realize the whole chipless sensor system, from the tag to the reader.

First, improving the sensitivity is a crucial point. Indeed we observed a delta RCS of 0.5 dB, for CO2 detection. This value of 0.5 dB is extracted from a difference between −28dBsm and −27.5dBsm. This weak difference is a limiting factor for the detection range. The other key parameter which limits the detection range is the sensitivity of the receiver and the noise floor of the first amplification stage. Using the radar equation, for the maximum allowed transmitting power (Pteirp = 36dBm), with a 6dBi receiving antenna, for a variation from −28dBsm to −27.5dBsm, we can measure a power variation of −18.4dBm at 20cm, −46.4dBm at 1m. This sensitivity can been achieved by commonly used power detectors, provided that the noise floor is below these values.

What is more problematic is the time–varying background noise due to mobile objects in the detection environment. Thus, with this current design, the detection area has to be isolated from these unwanted effects, which is the case when the sensors are used in a confined area.

To overcome this issue, the ideas listed below will be tested in a future work:

1) One technique consists in increasing the sensitive surface while keeping the same ratio Length/width to achieve the same bridging resistance.
2) Another idea is to change the formulation of the ink. Indeed, increasing the CNT concentration may enhance the sensitivity due to the higher number of sensitive elements for the same surface of composite ink.
3) The last idea is to align the CNTs using a magnetic or an electric field before sintering the ink.

The second major issue to overcome is to make a tag selective to only one parameter. Using several resonators loaded with different material can provide a higher selectivity if each resonator has a proper and unique behavior when subject to physical parameter. Indeed, based on measurement results, we can extract a multi-linear regression model between the various measured reflected power and resonant frequencies as input, and the temperature as well as the gas concentration as outputs. A similar technique has been successfully implemented in [20].

Last but not least, to improve the detection reliability in order to allow for a practical implementation of this technology in time-varying environments, one possible solution is to improve the design of resonators with the help of depolarizing scatterers as reported in [10]. In this case, the calibration procedure is not needed so that the sensor can be detected in a much larger area. Additionally, with depolarizing scatterers it becomes possible to detect a sensor when placed in contact with a metallic object or a container filled with liquids.

VI. Conclusion

In this paper, we introduced a flexible chipless sensor and studied its sensitivity to CO_2 and temperature. A solution to make this sensor sensitive only to temperature is proposed. It relies upon the deposition of a top coating layer. We demonstrated the realization of a fully inkjet-printed sensing platform realized with three different inks, namely:

1) Silver based nanoparticles ink (Harima Nanopaste) to realize the conductive strips.
2) Conductive organic SWCNT/PEDOT-PSS based ink (Poly-ink) to realize the sensitive strip.
3) Dielectric polymer based ink (PolyPrimer) to allow the temperature sensitivity only.

A parametric study done in simulation and confirmed by measurements, varying the resistivity of the sensitive strip allowed finding the optimal number of layers to maximize the linear and the logarithmic variation. Wireless measurement of the sensor subjected to a CO_2 concentration of 20000 ppm showed a variation of 0.5 dB and 0.2 dB without and with dielectric coating, respectively. Besides, we recorded magnitude shifts close to 2 dB for the different samples for a temperature variation from 60 °C to 30 °C. The top coating layer in this case doesn't attenuate the temperature sensitivity of the sensors. The measurements performed on several samples prove that sensors realized the same way have a very close behavior with each other. The next step is to implement these sensors as threshold detectors in a real environment. Further, another approach will be to implement these sensors on low cost substrates such as paper.

Acknowledgment

The authors would like to thank NEDO Japan and the National Science Foundation.

References

[1] S. Manzari, C. Occhiuzzi, S. Nawale, A. Catini, C. Di Natale, and G. Marrocco, "Polymer-doped UHF RFID tag for wireless-sensing of humidity," in *Proc. IEEE Int. Conf. RFID*, Orlando, FL, USA, Apr. 2012, pp. 124–129.

[2] R. Bhattacharyya, C. Floerkemeier, S. Sarma, and D. Deavours, "RFID tag antenna based temperature sensing in the frequency domain," in *Proc. IEEE Int. Conf. RFID*, Apr. 2011, pp. 70–77.

[3] C. S. Hartmann, "A global SAW ID tag with large data capacity," in *Proc. IEEE Ultrason. Symp.*, Oct. 2002, vol. 8, pp. 653–656,

[4] R. Nair, E. Perret, and S. Tedjini, "Temporal multi-frequency encoding technique for chipless RFID applications," in *IEEE MTT-S Int. Microw. Symp. Dig. (MTT)*, Jun. 2012, pp. 1–3.

[5] J. McVay, A. Hoorfar, and N. Engheta, "Space-filling curve RFID tags," in *Proc. IEEE Radio Wireless Symp.*, San Diego, CA, USA, Jan. 2006, pp. 199–202.

[6] S. Preradovic and N. C. Karmakar, "Multiresonator based chipless RFID tag and dedicated RFID reader," in *IEEE MTT-S Int. Microw. Symp. Dig.*, Anaheim, CA, USA, May 2010, pp. 1520–1523.

[7] H.-S. Jang, W.-G. Lim, K.-S. Oh, S.-M. Moon, and J.-W. Yu, "Design of low-cost chipless system using printable chipless tag with electromagnetic code," *IEEE Microw. Wireless Compon. Lett.*, vol. 20, no. 11, pp. 640–642, Nov. 2010.

[8] F. Costa, S. Genovesi, and A. Monorchio, "A chipless RFID based on multiresonant high-impedance surfaces," *IEEE Trans. Microw. Theory Techn.*, vol. 61, no. 1, pp. 146–153, Jan. 2013.

[9] A. Vena, A. A. Babar, L. Sydanheimo, M. M. Tentzeris, and L. Ukkonen, "A novel near-transparent ASK-reconfigurable inkjet-printed chipless RFID tag," *IEEE Antennas Wireless Propag. Lett.*, vol. 12, pp. 753–756, Jun. 2013.

[10] A. Vena, E. Perret, and S. Tedjni, "A depolarizing chipless RFID tag for robust detection and its FCC compliant UWB reading system," *IEEE Trans. Microw. Theory Techn.*, vol. 61, no. 8, pp. 2982–2994, Aug. 2013.

[11] L. Yang, R. Zhang, D. Staiculescu, C. P. Wong, and M. M. Tentzeris, "A novel conformal RFID-enabled module utilizing inkjet-printed antennas and carbon nanotubes for gas-detection applications," *IEEE Antennas Wireless Propag. Lett.*, vol. 8, pp. 653–656, May 2009.

[12] L. Taoran, V. Lakafosis, L. Ziyin, C. P. Wong, and M. M. Tentzeris, "Inkjet-printed graphene-based wireless gas sensor modules," in *Proc. IEEE 62nd Electron. Compon. Technol. Conf. (ECTC)*, May/Jun. 2012, pp. 1003–1008.

[13] T. Thai *et al.*, "Design and development of a millimetre-wave novel passive ultrasensitive temperature transducer for remote sensing and identification," in *Proc. Eur. Microw. Conf. (EuMC)*, Sep. 2010, pp. 45–48.

[14] A. Traille *et al.*, "A wireless passive RCS-based temperature sensor using liquid metal and microfluidics technologies," in *Proc. 41st Eur. Microw. Conf.*, Manchester, U.K., Oct. 2011, pp. 45–48.

[15] B. Kubina, C. Mandel, M. Schussler, M. Sazegar, and R. Jakoby, "A wireless chipless temperature sensor utilizing an orthogonal polarized backscatter scheme," in *Proc. 42nd Eur. Microw. Conf. (EuMC)*, Oct./Nov. 2012, pp. 61–64.

[16] E. M. Amin, S. Bhuiyan, N. Karmakar, and B. Winther-Jensen, "A novel EM barcode for humidity sensing," in *Proc. IEEE Int. Conf. RFID*, Apr./May 2013, pp. 82–87.

[17] C. Mandel, M. Schussler, and R. Jakoby, "A wireless passive strain sensor," in *Proc. IEEE Sensors*, Oct. 2011, pp. 207–210.

[18] A. Vena, L. Sydänheimo, M. M. Tentzeris, and L. Ukkonen, "A novel inkjet printed carbon nanotube-based chipless RFID sensor for gas detection," in *Proc. Eur. Microw. Conf.*, Nuremberg, Germany, Oct. 2013, pp. 9–12.
[19] Y. Wang and J. T. W. Yeow, "A review of carbon nanotubes-based gas sensors," *J. Sensors*, vol. 2009, pp. 493904-1–493904-24, May 2009.
[20] K. G. Ong, K. Zeng, and C. A. Grimes, "A wireless, passive carbon nanotube-based gas sensor," *IEEE Sensors J.*, vol. 2, no. 2, pp. 82–88, Apr. 2002.
[21] A. Firouzi, S. Sobri, F. M. Yasin, and F.-R. B. Ahmadun, "Fabrication of gas sensors based on carbon nanotube for CH_4 and CO_2 detection," in *Proc. Int. Conf. Nanotechnol. Biosensors (ICNB)*, Singapore, 2010.
[22] H. J. Yoon, D. H. Jun, J. H. Yang, Z. Zhou, S. S. Yang, and M. M. C. Cheng, "Carbon dioxide gas sensor using a graphene sheet," *Sens. Actuators B, Chem.*, vol. 157, no. 1, pp. 310–313, 2011.
[23] C. Hartmann, P. Hartmann, P. Brown, J. Bellamy, L. Claiborne, and W. Bonner, "Anti-collision methods for global SAW RFID tag systems," in *Proc. IEEE Ultrason. Symp.*, Aug. 2004, pp. 805–808.
[24] A. Denneulin, J. Bras, A. Blayo, B. Khelifi, F. Roussel-Dherbey, and C. Neuman, "The influence of carbon nanotubes in inkjet printing of conductive polymer suspensions," *Nanotechnology*, vol. 20, no. 38, p. 385701, 2009.
[25] *Poly-Ink*. [Online]. Available: http://www.poly-ink.fr/, accessed May 19, 2013.
[26] A. Denneulin, J. Bras, A. Blayo, and C. Neuman, "Substrate pretreatment of flexible material for printed electronics with carbon nanotube based ink," *Appl. Surf. Sci.*, vol. 257, no. 8, pp. 3645–3651, Feb. 2011.
[27] E. F. Knott, J. F. Shaeffer, and M. T. Tuley, *Radar Cross Section*, 2nd ed. Raleigh, NC, USA: SciTech Publishing, Inc., 2004.
[28] S. Preradovic, N. C. Karmakar, and M. Zenere, "UWB chipless tag RFID reader design," in *Proc. IEEE Int. Conf. RFID-Technol. Appl. (RFID-TA)*, Guangzhou, China, Jun. 2010, pp. 257–262.
[29] A. Ramos, D. Girbau, A. Lazaro, and S. Rima, "IR-UWB radar system and tag design for time-coded chipless RFID," in *Proc. 6th Eur. Conf. Antennas Propag. (EUCAP)*, Mar. 2012, pp. 2491–2494.

Arnaud Vena (M'13) received the Dipl.-Eng. degree in electrical engineering from the Institut National Polytechnique de Grenoble (Grenoble-INP), Grenoble, France, in 2005, and the Ph.D. degree from the Université de Grenoble, Grenoble, in 2012.

He joined ACS Solution France SAS in 2005, where he was responsible for the development of radio frequency identification (RFID) contactless card readers. In 2009, he started his research at Grenoble-INP, mainly involved in the design of chipless RFID systems. From 2012 to 2013, he held a post-doctoral position with the Tampere University of Technology, Tampere, Finland, in the field of conventional and chipless RFID sensors. Since 2013, he has been an Associate Professor of Electrical Engineering with the IES Laboratory, Université Montpellier 2, Montpellier, France. His current research interests are in the field of wireless sensors, RFID systems, and printed electronics.

Lauri Sydänheimo received the M.Sc. and Ph.D. degrees in electrical engineering from the Tampere University of Technology (TUT), Tampere, Finland. He is currently a Professor and Head of the Department of Electronics and Communications Engineering at TUT, and is the Research Director of the Rauma Research Unit with the Department of Electronics and Communications Engineering, TUT. He has authored over 170 publications in the field of radio frequency identification (RFID) tag and reader antenna design, and RFID system performance improvement. His research interests are focused on wireless data communication and RFID, in particular, RFID antennas and sensors.

Manos M. Tentzeris (S'89–M'92–SM'03–F'10) received the Diploma (*magna cum laude*) degree in electrical and computer engineering from the National Technical University of Athens, Athens, Greece, and the M.S. and Ph.D. degrees in electrical engineering and computer science from the University of Michigan, Ann Arbor, MI, USA. He is currently a Professor with the School of Electrical and Computer Engineering, Georgia Institute of Technology (Georgia Tech), Atlanta, GA, USA. He has published more than 480 papers in refereed journals and conference proceedings, five books, and 19 book chapters. He has helped to develop academic programs in Highly Integrated/Multilayer Packaging for RF and Wireless Applications using ceramic and organic flexible materials, paper-based radio frequency identifications (RFIDs) and sensors, biosensors, wearable electronics, inkjet-printed electronics, Green electronics and power scavenging, nanotechnology applications in RF, Microwave MEMs, SOP-integrated (UWB, multiband, mmW, and conformal) antennas, and heads the ATHENA research group (20 researchers). He is currently the Head of the GT-ECE Electromagnetics Technical Interest Group, and served as the Georgia Electronic Design Center Associate Director for RFID/Sensors research from 2006 to 2010 and as the Georgia Tech NSF-Packaging Research Center Associate Director for RF Research and the RF Alliance Leader from 2003 to 2006. He was a recipient/co-recipient of the 2012 FiDiPro Award in Finland, the iCMG Architecture Award of Excellence, the 2010 IEEE Antennas and Propagation Society Piergiorgio L. E. Uslenghi Letters Prize Paper Award, the 2011 International Workshop on Structural Health Monitoring Best Student Paper Award, the 2010 Georgia Tech Senior Faculty Outstanding Undergraduate Research Mentor Award, the 2009 IEEE TRANSACTIONS ON COMPONENTS AND PACKAGING TECHNOLOGIES Best Paper Award, the 2009 E. T. S. Walton Award from the Irish Science Foundation, the 2007 IEEE APS Symposium Best Student Paper Award, the 2007 IEEE IMS Third Best Student Paper Award, the 2007 ISAP 2007 Poster Presentation Award, the 2006 IEEE MTT Outstanding Young Engineer Award, the 2006 Asian-Pacific Microwave Conference Award, the 2004 IEEE TRANSACTIONS ON ADVANCED PACKAGING COMMENDABLE Paper Award, the 2003 NASA Godfrey Art Anzic Collaborative Distinguished Publication Award, the 2003 IBC International Educator of the Year Award, the 2003 IEEE CPMT Outstanding Young Engineer Award, the 2002 International Conference on Microwave and Millimeter-Wave Technology Best Paper Award (Beijing, China), the 2002 Georgia Tech-ECE Outstanding Junior Faculty Award, the 2001 ACES Conference Best Paper Award, the 2000 NSF CAREER Award, and the 1997 Best Paper Award of the International Hybrid Microelectronics and Packaging Society. He was the TPC Chair for the IEEE IMS 2008 Symposium and the Chair of the 2005 IEEE CEM-TD Workshop, and is the Vice Chair of the RF Technical Committee (TC16) of the IEEE CPMT Society. He is the founder and Chair of the RFID Technical Committee (TC24) of the IEEE MTT Society and the Secretary/Treasurer of the IEEE C-RFID. He is the Associate Editor of the IEEE TRANSACTIONS ON MICROWAVE THEORY AND TECHNIQUES, the IEEE TRANSACTIONS ON ADVANCED PACKAGING, and *International Journal on Antennas and Propagation*. He was a Visiting Professor with the Technical University of Munich, Munich, Germany, in Summer 2002, a Visiting Professor with GTRI-Ireland, Athlone, Ireland, in Summer 2009, and a Visiting Professor with LAAS-CNRS, Toulouse, France, in Summer 2010. He has given more than 100 invited talks to various universities and companies all over the world. He is a member of URSI-Commission D and MTT-15 committee, an Associate Member of EuMA, a fellow of the Electromagnetic Academy, and a member of the Technical Chamber of Greece. He was an IEEE MTT-S Distinguished Microwave Lecturer from 2010 to 2012.

Leena Ukkonen received the M.Sc. and Ph.D. degrees in electrical engineering in 2003 and 2006, respectively. She is currently a Professor with the Department of Electronics and Communications Engineering, Tampere University of Technology (TUT), Tampere, Finland, and is leading the Wireless Identification and Sensing Systems Research Group at the TUT Department of Electronics and Communications Engineering, Rauma Research Unit. She is an Academy of Finland Research Fellow and an Adjunct Professor with the Aalto University School of Science and Technology, Espoo, Finland. She has authored over 130 scientific publications in the fields of radio frequency identification (RFID) antenna design and industrial RFID applications. Her research interests are focused on RFID antenna development for tags, readers, and RFID sensors.